Analytical and Experimental Investigation of Laser-Microsphere Interaction for Nanoscale Surface Modification

Alex J. Heltzel

Senthil Theppakuttai

John R. Howell

Shaochen Chen

Department of Mechanical Engineering,
The University of Texas at Austin,
Austin, TX 78712

An analytical and experimental investigation on the features created on silicon by the irradiation of microspheres on the substrate surface with a pulsed laser is presented. Silica microspheres of 1.76 μm diameter are deposited on the silicon substrate and are irradiated with a pulsed Nd:YAG laser of wavelength 532 nm. An analytical model based on Mie theory is developed, which includes all evanescent terms and does not rely on either far-field or size-parameter approximations. The predicted intensity distributions on the substrate indicate a strong near-field enhancement confined to a very small area (nanometer scale). A multidimensional, numerical model was built to simulate the heat transfer through the silicon. An explicit scheme of the enthalpy method was employed to track the solid/liquid phase boundary. The experiment was performed for various laser energies used in the modeling, and the features obtained are characterized using a scanning electron microscope. The experimental results correlate well with the predicted results. [DOI: 10.1115/1.2039110]

Introduction

The industrial demand for smaller structures required for the manufacture of quantum devices, high-density recording media, etc., have resulted in the need for fabrication technology at the nanometer scale. Thus a variety of structuring techniques such as lithography [1] and focused ion beam patterning [2] have been investigated for nanofabrication. However, most of these techniques are limited either by their inability for large-area fabrication or by the diffraction limit and in most cases the high manufacturing costs.

To overcome the diffraction limit and to spatially control matter on a nanometer scale, several fabrication techniques based on near-field optics have been employed. One such technique for creating structures is utilizing the near-field radiation created around a microsphere by laser radiation. The accidental discovery of particle induced damage during dry laser cleaning of irregularly shaped Al_2O_3 particles on glass [3] has led to this exciting yet simple technique. When spherical colloidal particles such as silica (SiO_2) and polystyrene were used as contaminants on silicon wafers, features with diameters of 200–400 nm and depths of 10–80 nm depending on the irradiation conditions, were found at the former position of the particles. Instead of using colloidal particles, if microspheres are arranged in a periodic monolayer on the substrate, massively parallel nanostructuring could be realized [4].

In this paper, we study the nanofeatures created on silicon by irradiating 1.76 μm silica microspheres with a 532 nm pulsed Nd:YAG laser. The electromagnetic field surrounding the sphere is calculated using the exact solution presented by Mie [5]. The calculation does not rely on simplifying approximations used in limiting cases and previous attempts to describe the near field [6,7]. A phase change heat transfer model based on the enthalpy method was built to employ the enhanced laser intensity distributions. The

model predicts the resulting transient, two-dimensional temperature field in the silicon and the location of the moving phase boundary. To corroborate the predicted results, the microspheres are irradiated with different laser energies, and the features obtained experimentally are characterized by a scanning electron microscope (SEM).

Optical Field Modeling

The enhancement of incident intensity can be described from the starting point of Mie's theory of scattering. Born and Wolf [6] presents the rigorous solution to Maxwell's equations describing the scattered electromagnetic field components: $E_r^{(s)}$, $E_\theta^{(s)}$, $E_\phi^{(s)}$, $H_r^{(s)}$, $H_\theta^{(s)}$, $H_\phi^{(s)}$.

The coefficients eB_l and mB_l characterize the wave scattered by the sphere and are often simplified. The exact versions used for calculation in this paper are given by

$$eB_l = i^{l+1}\frac{2l+1}{l(l+1)}\frac{m\psi_l'(q)\psi_l(mq)-\psi_l(q)\psi_l'(mq)}{m\zeta_l^{(1)\prime}(q)\psi_l(mq)-\zeta_l^{(1)}(q)\psi_l'(mq)} \quad (1)$$

$$mB_l = i^{l+1}\frac{2l+1}{l(l+1)}\frac{m\psi_l(q)\psi_l'(mq)-\psi_l'(q)\psi_l(mq)}{m\zeta_l^{(1)}(q)\psi_l'(mq)-\zeta_l^{(1)\prime}(q)\psi_l(mq)} \quad (2)$$

The scattered electromagnetic field components are added to the incident field components (plane wave of the laser) to give the solution to Maxwell's equations both inside and outside the sphere. The parameter m is the complex refractive index of the sphere. The parameter q is equal to κ times the radius of the sphere, where κ is equal to 2π divided by the wavelength of the incident laser.

There is some difficulty associated with the exact calculation of the field components, specifically, the Bessel functions, Legendre functions, and their derivatives. Much of this difficulty can be circumvented by substituting asymptotic approximations for these terms that acceptably describe the field at a large distance from the particle. The critical coefficients eB_l and mB_l can be approximated for relatively large or highly conductive particles. In addition to individual term approximations, the overall intensity of the field is often approximated by squaring the amplitude of the electric vector. Under the conditions of the experiments presented, none of

these simplifications can be acceptably included. Most important, the far-field approximation cannot be utilized, as it is specifically the near-field enhancement that is assumed responsible for the substrate damage.

Because of the limitations, all terms in Mie's theory were calculated exactly up to the critical value of l_{cutoff}, after which the terms in the infinite sum were equal to zero. This was done through the use of recurrence relations for the Bessel functions and Legendre functions provided by [8,9]. The derivatives of these functions were determined numerically, with 45,000 values calculated in the range of $\theta = 0$ to $45°$, with the origin taken at the center of the sphere. The summation cutoff value of l was chosen to be

$$l_{cutoff} = \frac{2\pi an}{\lambda} + 4 \tag{3}$$

where a is the sphere radius, n is the real component of the refractive index of the sphere, and λ is the incident wavelength of the laser. An investigation was carried out to determine the effectiveness of the l_{cutoff} value. The magnitude of the real and imaginary coefficients, eB_l and mB_l, respectively, fell to zero through four decimal places by the final term included in the summation for all theoretical cases. Therefore, l_{cutoff} was chosen large enough to contain every term of value in the infinite series.

The intensity of the radiation incident on the plane of the substrate is quantified using the Poynting vector of the electromagnetic field. The spherical components of the time-averaged Poynting vector are

$$S_r = I_0 \, \mathrm{Re}[E_\theta H_\phi^* - E_\phi H_\theta^*]$$
$$S_\theta = I_0 \, \mathrm{Re}[E_\phi H_r^* - E_r H_\phi^*] \tag{4}$$
$$S_\phi = I_0 \, \mathrm{Re}[E_r H_\theta^* - E_\theta H_r^*]$$

where I_0 is the intensity of the incident laser, and the asterisk superscript indicates the complex conjugate of the magnetic field components. The z-direction is taken longitudinal to the incident laser and normal to the substrate lying beneath the particle. The z-component of the Poynting vector is therefore a description of the energy incident upon the substrate surface due to the laser and the presence of the microsphere. The coordinate convention used dictates the z-component equal to

$$S_z = \cos\theta \, S_r - \sin\theta \, S_\theta \tag{5}$$

The effect of secondary reflection of energy between the substrate and sphere boundaries is not accounted for in the S_z value. This is a potential source of error judging by the results of Luk'yanchuck et al. [7], who found an increase in peak enhancement due to substrate effect. However, the Mie calculations in [7] used for comparison neglected the magnetic field components, which were necessarily included in the present work. The Mie results corresponding to identical cases between [7] and this work differ by up to a factor of 4 in peak enhancement values.

The authors are conducting an investigation to determine the necessity of including secondary reflection on the overall heat transfer effect, which will be included in future work if found significant.

S_z has been calculated for certain cases available for experimentation. Figure 1 shows the intensity distribution on the substrate with parameters: $a = 0.88 \, \mu$m, $\lambda = 532$ nm, and $n = 1.37$, corresponding to a silica sphere 1.76 μm in diameter. The resulting peak intensity predicted is 14.65 times the incident intensity. A fraction of this energy will be reflected to the environment. At this wavelength, the fluence required to damage the substrate is in the range of $600-650$ mJ/cm^2. Theoretically, the enhancement predicted by the model would lower the input energy threshold to roughly $40-45$ mJ/cm^2.

Figure 2 is a cross section of Fig. 1 taken along one of the horizontal axes through the contact point of the sphere and sur-
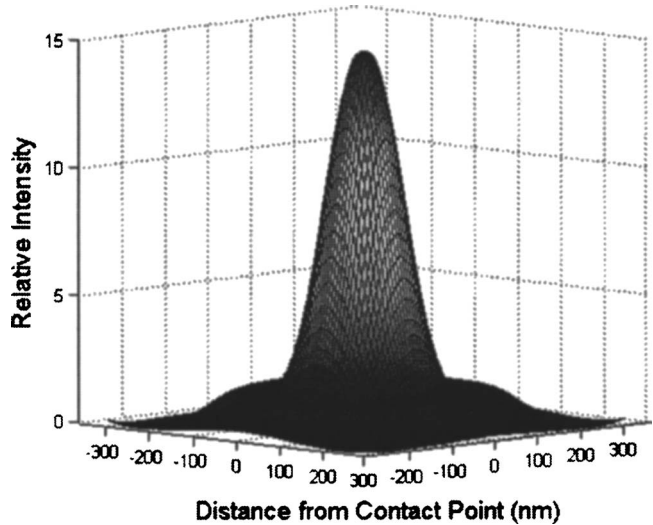
Fig. 1 Intensity enhancement on silicon surface due to laser-microsphere interaction: $\lambda = 532$ nm, silica microsphere 1.76 μm in diameter

face. It is evident that for this case, the predicted enhancement is concentrated within a circular area on the substrate surface with radius less than 200 nm.

Figure 3 illustrates the predicted dependence of the enhancement effect on the proximity of the sphere to the surface. S_z was calculated with the sphere moved a single radius away from the surface. The predicted enhancement decreases dramatically and is focused to a lesser degree with the area directly under the sphere.
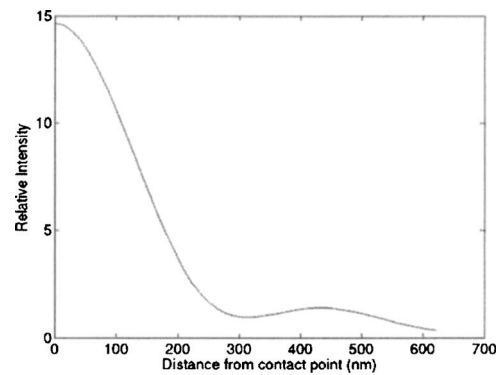
Fig. 2 Intensity enhancement on silicon from 1.76 μm SiO$_2$ spheres and 532 nm laser
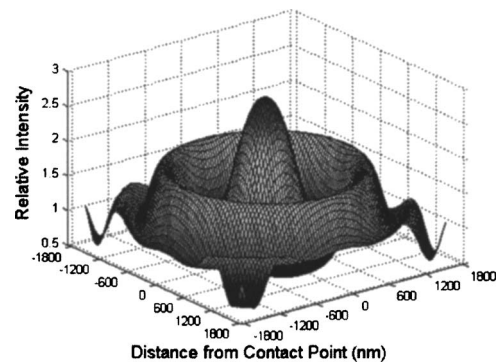
Fig. 3 Intensity enhancement on silicon substrate from 1.76 μm diameter silica particle elevated 1.76 μm above surface, 532 nm laser

The secondary and tertiary "waves" of intensity are relatively more significant compared to Fig. 1, and effectively average to unity outside the primary enhancement. The peak enhancement resulting from the Mie calculation is again at the contact point, but this magnitude deviates between cases. At certain distances from the substrate the secondary ring may actually represent the peak near-field enhancement.

Modeling of Heat Transfer in the Substrate

Calculation of the laser intensity enhancement provides a boundary condition to employ in a model of the heat transfer within the substrate. The goal of the simulation is to obtain the temperature and phase (solid/liquid) distribution in the silicon, which indicates the size and shape of the melt zone. This data are then compared with experimental observations characterized using a SEM.

The ~6 ns duration of the laser pulse allows the use of Fourier conduction within the substrate, which is modeled as a semi-infinite slab. The enthalpy method was used explicitly to account for the moving phase boundary within the material (Stefan problem) [10–12]. The heat equation as a function of the enthalpy in the solid silicon is

$$\rho \frac{\partial h}{\partial t} = \frac{\partial}{\partial x}\left(k\frac{\partial T}{\partial x}\right) + \frac{\partial}{\partial y}\left(k\frac{\partial T}{\partial y}\right) + \dot{q} \tag{6}$$

with the generation term $\dot{q}(\text{W/m}^3)$ is equal to

$$\dot{q} = (1-R)q_{inc}(x_{int},t)\gamma e^{(-\gamma z)} \tag{7}$$

where R is the reflectivity of silicon dependent on the wavelength of the incident light and phase of the silicon, and γ is the absorption coefficient, given by

$$R = \frac{(n-1)^2 + k_x^2}{(n+1)^2 + k_x^2} \tag{8}$$

$$\gamma = \frac{4\pi k_x}{\lambda} \tag{9}$$

q_{inc} is the enhanced value of laser energy taken at x_{int}, the surface intercept node between the node in the solid and the center of the sphere. It follows a Gaussian shape through time given by

$$q_{inc}(x_{int},t) = A\exp[-(B-t)^2/C]I(x_{int}) \tag{10}$$

The constants B and C are fit to the laser wave form, while A ensures the total energy incident corresponds to the proper fluence, and $I(x_{int})$ refers to the intensity distribution in Fig. 1.

New values of h are calculated explicitly every time step, relying only on the surrounding temperatures from the previous iteration. This precludes the need to invert matrices or employ other convergence algorithms, but requires the following expression to be obeyed to prevent divergence of the solution.

$$\frac{\Delta t}{\Delta x^2} \leq \frac{\rho c}{2k} \tag{11}$$

This expression limits the numerical time and space steps in terms of the specific heat, density, and thermal conductivity of the material. Using the extreme values of all three variables in the anticipated temperature range, the left-hand side of (11) must be less than approximately 6000. Time steps of 75 fs and space steps of 19.5 nm were used to obtain the following results, and were proven adequate by grid-independence investigations.

At the surface of the substrate in the presence of opaque liquid silicon, an energy conserving boundary condition is used to account for energy loss due to radiation, which was found to be significant.

$$(1-R)q_{inc} - \varepsilon\sigma T^4 = k\frac{\Delta T}{\Delta y} + \rho c\Delta y\frac{\Delta T}{\Delta t} \tag{12}$$
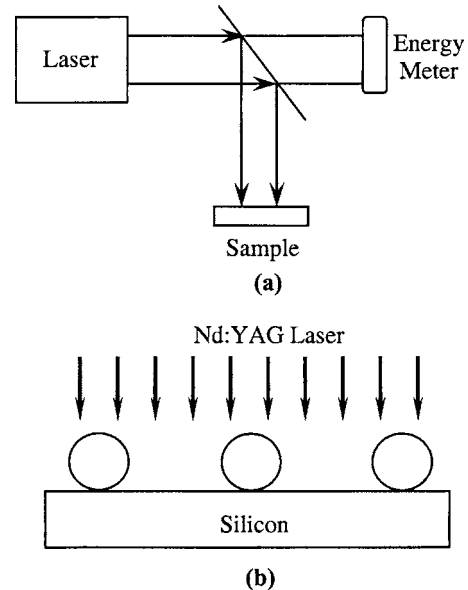
Fig. 4 Laser irradiation of disperse silica spheres on silicon substrate: (*a*) Schematic of the experimental setup; (*b*) schematic of silica microspheres on silicon

The emissivity ε of the liquid silicon is determined from the following relation

$$\varepsilon(\lambda,T) = \frac{4n}{n^2 + k_x^2 + 2n + 1} \tag{13}$$

where the refractive indices n and k_x are obtained from [13,14].

The new value of calculated enthalpy determines the temperature at the node based on the following relations

$$T_{x,y}^{t+1} = h_{x,y}^{t+1}/c_l, \quad h^{t+1} < (cT_m)$$

$$T_{x,y}^{t+1} = T_m, \quad (cT_m) < h^{t+1} < (cT_m + L) \tag{14}$$

$$T_{x,y}^{t+1} = (h_{x,y}^{t+1} - (c-c_l)T_m - L_m)/c_l, \quad h^{t+1} \geq (cT_m + L)$$

The silicon is therefore separated into three regimes: solid, liquid, and a transition zone. The boundaries of these regions are tracked through time using the preceding method.

Experimental Setup

The sample used for patterning is a 500 μm thick *n*-type (100) polished silicon wafer with a surface roughness of a few nanometers (<2 nm) and a 2–3 nm thick native oxide layer. Before processing the sample, care was taken to ensure that the sample is clean and free of any contaminants. For this reason, it is first cleaned in ethanol solution followed by rinsing in deionized water. After the sample is dried with nitrogen gas, a colloidal suspension of mono-dispersed silica spheres diluted with deionized water is applied on the glass sample and let to dry [15].

The schematic of our experimental setup is shown in Fig. 4(*a*). The output from a pulsed Nd:YAG laser passes through a beam splitter, which splits the incident laser beam into two: one part for patterning and the other for measuring the laser energy. The sample is mounted on a three-dimensional stage and the laser beam is focused onto the sample by using a plano-convex lens.

A single pulse from the laser is incident on the spheres as shown in Fig. 4(*b*). Since the sphere is immediately on top of the substrate, the incident laser beam induces a near-field around the sphere. This enhanced field is responsible for the formation of nanofeatures on the silicon substrate. The features thus obtained were characterized using an SEM and are presented in the results and discussion section of the paper.
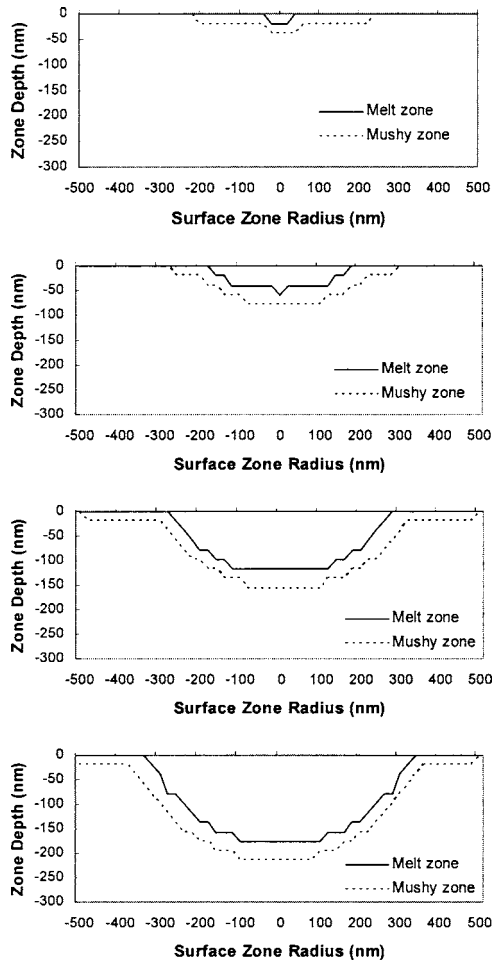
Fig. 5 Predicted geometry of melt and mushy zones in silicon at laser fluence of (*a*) 50 mJ/cm^2, (*b*) 100 mJ/cm^2, (*c*) 200 mJ/cm^2, and (*d*) 300 mJ/cm^2

Fig. 6 SEM micrograph of 1.76 μm SiO$_2$ spheres irradiated by 532 nm laser at a fluence of (*a*) 50 mJ/cm^2, (*b*) 100 mJ/cm^2, (*c*) 200 mJ/cm^2, and (*d*) 300 mJ/cm^2

Results and Discussion

The heat transfer simulations were conducted using 1.76 μm SiO$_2$ spheres irradiated by a single 532 nm laser pulse at four fluences: 50, 100, 200, and 300 mJ/cm^2. The boundary condition of Figure 2 employed in Eq. (10) was used in all cases. Figure 5 gives the numerical results predicting the width and depth of the melt and mushy zones in the silicon for the four laser energies.

There are essentially two points of comparison available between the SEM micrographs and the simulation results: the size of the surface damage, and the threshold energy below which no damage occurs. At 50 mJ/cm^2, the model predicts that the surface of the substrate barely reaches the melting temperature, with melt zone only a few nm wide and deep, and a mushy or heat-affected zone approximately 430 nm wide. The heat affected zone is very shallow, and in terms of transience the melting temperature is only attained for a few nanoseconds. At 100 mJ/cm^2, the model predicts a melted zone approximately 332 nm in diameter, which a total heat affected region of 548 nm diameter. At 200 mJ/cm^2, a zone of melted silicon 528 nm in diameter is predicted, with a heat affected region 939 nm in diameter. Here the predicted melt depth doubles to 156 nm. At energy of 300 mJ/cm^2, a zone of melted silicon approximately 645 nm with a total heat affected zone of 958 nm in diameter is predicted. A melt depth of 215 nm is also predicted.

Figure 6 is a SEM micrograph of the silicon substrate after irradiation of the silica spheres at different laser fluences. At fluences of 200 and 300 mJ/cm^2 the diameter of the features ob-

tained are ~1000 nm, matching the predictions perfectly. However at 50 mJ/cm^2 and 100 mJ/cm^2 the size of the zone shrinks, but not quite to the degree predicted numerically. It can also be observed that some of the features obtained are not perfectly circular as predicted. This is mainly because of the slight variation in the laser incident angle due to the beam delivery optics used in the experiment. A direct comparison of the feature diameters between the predicted and experimental results is presented in Fig. 7.

Both the extent of the surface modification and the damage threshold predicted are very close to what is observed experimentally. The experimental results show very little damage to the substrate when the particles are irradiated at a fluence of 50 mJ/cm^2, and by comparing with the modeling results it is evident that this energy is very close to the threshold below which no damage to silicon occurs. An additional simulation was conducted at a fluence of 40 mJ/cm^2, which returned a peak temperature below the melting point of silicon. This is a strong indication that the level of enhancement obtained from the electromagnetic field calculations is accurate.

Conclusion

Features created on a silicon substrate by the irradiation of microspheres on a silicon substrate surface with a pulsed laser have been presented. The features indicate an enhancement of the incident intensity in the near field due to the presence of the sphere. The near field has been calculated for a single sphere on a substrate using the results of Mie theory without relying on any simplifying approximations. The results of these calculations predict a strong enhancement directly under the sphere, which is assumed to be responsible for the substrate damage. A numerical model was built to simulate the heat transfer through the silicon substrate and track the phase change boundary through time. The dominant
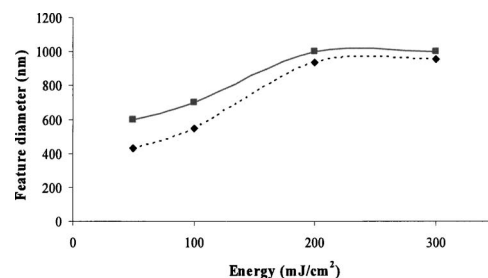
Fig. 7 Comparison of the predicted and experimental feature diameters for 1.76 μm SiO$_2$ spheres irradiated by 532 nm laser at different laser fluences

modes of heat transfer employed were radiation absorbed in the solid volume, radiation emitted from the surface, and conduction through the volume. The results of the modeling correlate well with the substrate damage characterized with a SEM. The threshold energy required to damage the substrate with the presence of microspheres matches the level of enhancement predicted by the Mie theory calculations.

Acknowledgments

Nomenclature

A = sphere radius
A, B, C = constants describing laser wave form, Eq. (10)
E = electric field vector
H = magnetic field vector
I_o = incident laser intensity
L = enthalpy of fusion
R = surface reflectivity
S = Poynting vector
T = temperature, K
c = specific heat of substrate
eB = wave scattering coefficient, Eq. (1)
h = enthalpy of substrate material
k = thermal conductivity of substrate material
k_x = imaginary refractive index component
mB = wave scattering coefficient, Eq. (2)
n = real refractive index component
q = κa
q_{inc} = laser energy incident on substrate
q = volumetric energy generation rate, W/m^3
r = radial coordinate
t = time
x, y, z = Cartesian coordinates in substrate
γ = absorption coefficient, Eq. (9)
ε = emissivity of liquid substrate surface, Eq. (13)
θ = spherical coordinate
κ = $2\pi/\lambda$
λ = wavelength
ρ = density of substrate material
ϕ = spherical coordinate

Subscripts

$cutoff$ = value at limit of summation, Eq. (8)
inc = incident
l = liquid phase
m = value at the melting point
x = in the x-direction

Superscripts

$*$ = complex conjugate

References

[1] Dial, O., Cheng, C. C., and Scherer, A., 1998, "Fabrication of High-Density Nanostructures by Electron Beam Lithography," J. Vac. Sci. Technol. B, **16**, pp. 3887–3890.
[2] Terris, B. D., Weller, D., Folks, L., Baglin, J. E. E., and Kellock, A. J., 2000, "Patterning Magnetic Films by Ion Beam Irradiation," J. Appl. Phys., **87**, pp. 7004–7006.
[3] Halfpenny, D. R., and Kane, D. M., 1999, "A Quantitative Analysis of Single Pulse Ultraviolet Dry Laser Cleaning," J. Appl. Phys., **86**, pp. 6641–6646.
[4] Lu, Y., Theppakuttai, S., and Chen, S. C., 2003, "Marangoni Effect in Nanosphere-Enhanced Laser Nanopatterning of Silicon," Appl. Phys. Lett., **82**, pp. 4143–4145.
[5] Mie, G., 1908, "Beitrage zur Optik Truber Medien Speziell Kolloidaler Metallosungen," Ann. Phys., **25**, pp. 377–445.
[6] Born, M., and Wolf, E., 1999, *Principles of Optics*, 7th ed., Cambridge University, Cambridge, England.
[7] Luk'yanchuck, B. S., Zheng, Y. W., and Lu, Y. F., 2000, "Laser Cleaning of Solid Surface: Optical Resonance and Near-Field Effects," Proc. SPIE, **4065**, pp. 576–587.
[8] Abramowitz, M., and Stegun, I., 1965, *Handbook of Mathematical Functions*, Dover, New York.
[9] Lowan, A., et al., 1945, *Tables of Associated Legendre Functions*, Columbia University Press, New York.
[10] Xu, X., Grigoropoulos, C. P., and Russo, R. E., 1995, "Heat Transfer in Excimer Laser Melting of Thin Polysilicon Layers," ASME J. Heat Transfer, **117**, pp. 708–715.
[11] Shamsundar, N., and Sparrow, E. M., 1975, "Analysis of Multidimensional Conduction Phase Change Via the Enthalpy Method," ASME J. Heat Transfer, **97**, pp. 333–340.
[12] Minkowycz, W. J., and Sparrow, E. M., 1996, *Advances in Numerical Heat Transfer*, Taylor and Francis Group, Washington, DC, Vol. 1.
[13] Jellison, G. E., 1987, "Measurements of the Optical Properties of Liquid Silicon and Germanium using Nanosecond Time-Resolved Ellipsometry," Appl. Phys. Lett., **51**, pp. 352–354.
[14] Hull, R., 1999, *Properties of Crystalline Silicon*, The Institute of Elec. Eng., London.
[15] Mosbacher, M., Chaoui, N., Siegel, J., Dobler, V., Solis, J., Boneberg, J., Afonso, C. N., and Leiderer, P., 1999, "A Comparison of ns and ps Steam Laser Cleaning of Si Surfaces," Appl. Phys. A: Mater. Sci. Process., **69**, pp. S331–S334.